

Supporting Information

Composite supraparticles with tunable light emission

Federico Montanarella^{†,‡}, Thomas Altantzis[§], Daniele Zanaga[§], Freddy T. Rabouw[‡], Sara Bals[§], Patrick Baesjou[‡], Daniel Vanmaekelbergh^{†} and Alfons van Blaaderen^{‡*}*

[†]Condensed Matter and Interfaces, Debye Institute for Nanomaterials Science, Utrecht University, P.O. Box 80000, 3508 TA Utrecht, The Netherlands

[‡]Soft Condensed Matter, Debye Institute for Nanomaterials Science, Utrecht University, P.O. Box 80000, 3508 TA Utrecht, The Netherlands

[§]EMAT, University of Antwerp, Groenenborgerlaan 171, B-2020 Antwerp, Belgium

EXPERIMENTAL SECTION

Chemicals

Sodium dodecyl sulfate (SDS, $\geq 98.5\%$), Dextran from *Leuconostoc mesenteroides* (Mw 670000 g/mol), Trioctylphosphine oxide (TOPO, 90%), Octadecylamine (ODA, 90%), Oleic acid (OA, 90%), 1-Octadecene (ODE, 90%), Cadmium acetate dihydrate ($\text{Cd}(\text{Ac})_2 \cdot 2\text{H}_2\text{O}$, 98%), Trioctylphosphine (TOP, 90%), Sulfur (S, 99.998%), Ethanol (EtOH, 99.8%), 1-Butanol anhydrous (BuOH, 99.8%), Methanol (MeOH, anhydrous, 99.8%), Toluene (anhydrous, 99.8%), Cadmium oxide (CdO, 99.99%), Zinc acetate dihydrate ($\text{Zn}(\text{Ac})_2$, $\geq 98\%$), 1-octanethiol ($\geq 98.5\%$), Chloroform ($\geq 99\%$) were all purchased by Sigma Aldrich and used as received. Se powder (Se, 200 mesh, 99.999%) and Diethylzinc (95%) were purchased from Brunshwig Chemie. Acetone (dried) was purchased by VWR International.

Synthesis of red emitting QDs

Synthesis of the precursors: Prior to the synthesis, different precursors were prepared. The Cd- and Se- precursors for the synthesis of the cores were prepared as follows. For the Cd- precursor, 51.84 g of ODE were mixed in a 100 mL Erlenmeyer with 7.36 g of OA and 1.28 g of $\text{Cd}(\text{Ac})_2 \cdot 2\text{H}_2\text{O}$. This solution was stirred at 150°C under vacuum in a schlenkline for two hours. For the Se- precursor, 4.25 g of Se were mixed with 22.5 g of TOP and 35.7 g of ODE in a 50 mL Erlenmeyer. The solution was stirred at 50°C until complete dissolution of the Se.

Synthesis of the cores: The synthesis was performed in a schlenkline under nitrogen atmosphere. In a 50 mL three neck flask, 2.22 g of TOPO, 6.40 g of ODA and 9.8 g of Cd

precursor solution were mixed, and the temperature was increased to 300°C. When this temperature was reached, 10.4 g of Se precursor solution was quickly injected in the mixture. The nanocrystals were allowed to grow for 30 s, after which the solution was rapidly cooled down to room temperature with the aid of compressed air. The particles were diluted by adding 1 equivalent of hexane. The NCs were then washed by adding 2 equivalents of MeOH and collecting the upper colored layer of the resulting two-phase system. The NCs were then precipitated by adding 1 equivalent of acetone and centrifuging at 2500 rpm for 5 min. The NCs were finally redispersed in 10 mL of toluene and stored inside the glovebox.

Growth of CdS shells: This synthesis was adapted from another procedure¹ from literature. Prior to the synthesis, the Cd-, S- and Zn- precursors were prepared. For the Cd- precursors, 5.5 g of Cd(Ac)₂·2H₂O were mixed with 54.15 g of OA and 216 mL of ODE in a 500 mL Erlenmeyer. The mixture was stirred for 2 hours at 120 °C under vacuum. For the S- precursor, 0.320 g of S was mixed with 100 mL of ODE in a 250 mL Erlenmeyer and heavily stirred at 180 °C until complete dissolution of the S. For the Zn- precursor, 0.988 g of diethylzinc was mixed with 40 mL of ODE in a 100 mL Erlenmeyer in a glovebox. The mixture was stirred at room temperature while 10.10 mL of OA was added dropwise. The solution started foaming and was kept stirring until complete stabilization; at that point the temperature was increased to 310 °C and the solution was further stirred for 5 min.

For the growth of CdS shells, $1 \cdot 10^{-7}$ M of NCs (3.1 nm in diameter) in toluene solution were combined with 5 g of ODE and 1.5 g of ODA. The solution was stirred at 150 °C for 1 hour in order to let all the toluene evaporate. The reaction temperature was then increased to 240 °C and,

in steps with reaction periods of 30 min, the precursors were added slowly to grow the shell layer by layer. In total, 10 monolayers of CdS, 2 monolayer of CdZnS and 2 monolayer of ZnS were grown.

Monlayer #	Precursor to add (mL)		
	S	Cd/Zn	
0	-	-	-
1	0.143	0.143	Cd
2	0.181	0.181	Cd
3	0.223	0.223	Cd
4	0.270	0.270	Cd
5	0.321	0.321	Cd
6	0.377	0.377	Cd
7	0.438	0.438	Cd
8	0.502	0.502	Cd
9	0.572	0.572	Cd
10	0.645	0.645	Cd
11	0.723	0.723	Cd/Zn
12	0.806	0.806	Cd/Zn
13	0.893	0.893	Zn
14	0.895	0.895	Zn

After the growth, the reaction mixture was cooled down to room temperature and diluted by adding 1 equivalent of toluene. The NCs were washed by adding 2 equivalents of a 1:2 v/v BuOH:MeOH mixture, then centrifuging at 2500 rpm in order to precipitate the NCs, and then redispersing the pellet in 10 mL of toluene. The NCs were stored in the glovebox under nitrogen atmosphere.

Synthesis of green emitting QDs

The synthesis procedure was adapted by a protocol found in literature.² For the synthesis, 0.2 mmol (2.7 mg) of CdO, 4 mmol (878.0 mg) of Zn(Ac)₂ and 5 mL of OA were mixed in a 100 mL three neck bottle in a schlenkline. The mixture was stirred for 30 min under vacuum at 150

°C in order to degas. Then 15 mL of ODE was added. The temperature was then increased to 310°C under nitrogen, thus obtaining clear solution. Then a solution composed of 0.2 mmol (15.8 mg) of Se, 4 mmol (128.3 mg) of S and 2 mL of TOP, previously stirred at 70°C until complete dissolution, was rapidly injected in the reaction bath. The solution quickly changed color to orange and the NCs were allowed to grow for 10 min at 300 °C. After this time, 0.5 mL of 1-octanethiol were added in order to passivate the surfaces of the NCs. The solution was further stirred for 5 min, then it was let cool down to room temperature, where it looked yellow. The NCs were finally washed twice by adding 1 equivalent of chloroform, precipitating by adding 2 equivalents of acetone and then centrifuging at 2500 rpm. The NCs were finally redispersed in 5 mL of toluene.

Synthesis of blue emitting QDs

The procedure was adapted from a protocol found in literature.³ The synthesis was performed in a schlenkline in nitrogen atmosphere. For the synthesis, 1 mmol (128.4 mg) of CdO, 10 mmol (1.83 g) of Zn(Ac)₂ and 7.0 mL of OA were mixed and stirred in a three neck bottle at 150 °C, under vacuum, for 40 min, obtaining a pale yellow solution. Then 15 mL of ODE was added and the mixture was heated up at 310 °C under nitrogen atmosphere. When the temperature was reached, a solution made of 1.6 mmol (51 mg) of S and 2.4 mL of ODE, previously mixed at 70 °C to complete dissolution, was quickly injected in the reaction bath, obtaining a vivid yellow solution. The mixture was left to react for 12 min, after which another solution, made of 4 mmol (128.1 mg) of S and 5 mL of OA, previously mixed at 70°C upon complete dissolution, was injected at a speed of 0.5 mL/min in the reaction bath, obtaining a dark orange solution. The mixture was left to react for 3 hours, after which it was cooled down to room temperature by

removing the heating source. The solution was washed by adding 2 equivalents of EtOH and centrifuging at 2500 rpm, in order to precipitate the NCs. The NCs were then redispersed in toluene and washed another time with a 1:1 v/v BuOH:MeOH solution, centrifuging at 2500 rpm and redispersing the pellet in 10 mL of toluene.

Characterization of the separate NC batches

The red emitting NCs consist of a 3.1 nm CdSe core with 5 monolayers (ML) of CdS, 1 ML of CdZnS and 1 ML of ZnS. These core/multi-shell NCs are nearly spherical with a diameter of 10.3 ± 1.0 nm, and the PL emission is centered at 627 nm. The measured photoluminescence quantum yield (QY) is 75 %. The green emitting NCs were obtained by a single-step synthesis and consist of an alloyed core-shell structure of CdSe at the center and ZnS at the surface with a graded interface. The NCs have a diameter of 11.0 ± 1.1 nm, the PL emission is centered around 512 nm and the QY was measured to be 81%. The blue emitting NCs were also synthesized using a single-step method and consist of an alloyed structure with a CdZnS core and a ZnS shell with a graded interface. The final NCs have an irregular shape with a size of 10.5 ± 1.3 nm. The PL emission is centered at 477 nm with a QY of 12%. The synthesis procedure of the three NC components has been adjusted in order to get a thick shell around the core. This results not only in excellent photochemical stability, but also in a pronounced separation in energy between the dominant absorption feature coming from the massive NC shell and the luminescence from the core. In such a way, reabsorption of the red and green emission, and also partially of the blue emission can be largely reduced when the different NCs are present in mixed suspensions or in the SPs.

Synthesis of SPs

The synthesis was performed in open air. First of all, the three different populations of NCs, dispersed in cyclohexane, were premixed in the desired ratios forming 1 mL of mixed solution. The solution with volume fractions on the order of 10% of NCs was emulsified with a water solution made of 10mL of milli-Q water containing 60mg of sodiumdodecylsulfate (SDS), the surfactant, and 0.4g of dextran. Dextran acts as steric stabilizer, but is also added as well to bring the solution in a visco-elastic regime necessary for creating relatively monodisperse droplets under high shear rates.⁴ Then, the water solution and the oil solution were brought in contact, thus forming a two phase system. This system was then emulsified. The emulsification, together with the initial volume fraction of particles, is important, since it will determine the size of the droplets and consequently, after the evaporation of the oil phase, the mean size and size distribution of the resulting SPs. We used two methods to realize our emulsions, both allowing relatively easy scaling up: sonication and a methodology developed by the Bibette group that uses high shear rates generated in a Couette shear cell.⁵ In the sonication process, ultrasonic waves were used in order to break the two phase system in a emulsion. This method resulted in a relatively polydisperse emulsion (PD ~ 20%) consisting of medium-size SPs with diameters in a size range between 500 nm (size distribution: ± 100 nm) and 2 μ m (size distribution: ± 400 nm). SPs in Fig. 3 in the main text and S9 of the SI were made using this method. Using the shear method developed by Bibette *et al.* control over the average size of the particles and the resulting polydispersity are better. In fact SPs with a precise size, in a size range between 100 nm and 500 nm, can be produced with control over the size (Fig.S2) by changing the shear rate during the emulsification. These values for the size range are more restrictive compared to the ones cited by Bibette *et al.*, but in our case we limited ourselves to these sizes by using an initial volume

fraction of 10% and, thus, an initial droplet size of 2-3 μm . As mentioned, the shear procedure gave better results in terms of polydispersity (PD \sim 15%) and, as sonication, it is also quite rapid, taking just few minutes, and for this reason it was the most used in our experiments. SPs in Fig. 2 in the main text and S2, S3, S4, S5 and S8 of the SI were made using this method. After the emulsification, the emulsion was then collected and stirred for 4 hours at 68°C, in order to evaporate the oil phase (=cyclohexane). The resulting dispersion was centrifuged at 2000 rpm for 10 min, and the sedimented SPs were finally redispersed in distilled water.

Optical Measurements

The PL quantum yield (PLQY) measurements were performed on samples consisting of diluted NC or SP solutions (cyclohexane for NCs, Milli-Q water for SPs) in a quartz cuvette using an Edinburgh instruments F900 spectrometer with an integrating sphere and excitation at 420 nm. The measured PLQY for our composed SPs is up to 25%. When going from solution of NCs in toluene to SPs of one single population of NCs, the measured PLQY changes as follow: for SPs composed of only red emitting NCs the PLQY remains stable at 75%, for SPs composed of only green NCs the PLQY goes from 81% to 40%, and for SPs composed of only blue emitting NCs the PLQY goes from 12% to 2%.

Confocal images were acquired with a Leica SP8 confocal microscope fitted with a pulsed super continuum source (NKT Photonics, 400 nm, 5 ps pulse duration, 78 MHz repetition rate), focusing objective (100x /1.4 NA oil-immersion confocal objective (LEICA), and PMT detection. The investigated individual supraparticles were lying on a 600 nm SiO₂ covered Si substrate, 0,15 mm thick, and immersed in Leica immersion oil type F.

The images taken with the confocal microscope were processed by deconvolution using the point spread function (PSF) of the microscope, which was recently determined experimentally (width 190 nm in the x - y imaging plane and 490 nm along the optical z -axis⁶), and were deconvoluted afterwards. We note, however, that the images might be slightly distorted by the large refractive index contrast between the SPs and the surrounding environment.

PL emission and decay traces were recorded using an Edinburgh instruments F900 spectrometer, while absorption was measured with a PerkinElmer lambda 950 spectrophotometer.

Analysis of photoluminescence decay dynamics

The photoluminescence decay curves of Figure 4b–d in the main text were measured after spectrally selecting the relevant emission using a grating and slit. From the often multi-exponential curves we fitted the acceleration of decay upon assembly of the NCs into a SP without assuming any particular functional form for the curves (e.g. mono-exponential, bi-exponential, stretched exponential, or a log-normal rate distribution). Instead, we determined the optimal acceleration factor x that could shift the decay curve of the individual NCs onto those of the SPs through a transformation $t \rightarrow t/x$ of the time coordinates of the data points. This yields an acceleration of 66% upon going from individual red NCs to SPs purely consisting of red NCs, and an acceleration of 34% upon going to mixed (white-light emitting) SPs. For green NCs these numbers are 41% and 32%, and for blue NCs 29% and 211%.

To benchmark this analysis method, we can compare it to more conventional single-exponential fitting on the data of the red NCs. (Note however that such fits match the data poorly in case of multi-exponential decay curves). Using single-exponential fitting on the first 100 ns, the accelerations would be estimated as $(39 \text{ ns} / 24 \text{ ns} - 1) = 63\%$ and $(39 \text{ ns} / 31 \text{ ns} - 1) = 23\%$ for the red NCs; $(20 \text{ ns} / 31 \text{ ns} - 1) = 40\%$ and $(20 \text{ ns} / 16 \text{ ns} - 1) = 21\%$ for the green NCs; and $(14 \text{ ns} / 8 \text{ ns} - 1) = 68\%$ and $(14 \text{ ns} / 5 \text{ ns} - 1) = 197\%$ for the blue NCs. The results of the two methods are qualitatively the same.

Definition of polydispersity

All the values of sizes in the article are given with the mean (μ) and the standard deviation (σ) in the form: $\mu \pm \sigma$. Polydispersity of size is defined as $PD (\%) = \frac{\sigma}{\mu} \cdot 100$.

Hydrodynamic diameter

The hydrodynamic diameter (*i.e.* the diameter of the semiconductor material plus the ligand shell) of the particles has been precisely measured for the red population of NCs, characterized by a spherical shape and therefore easier to analyze, from visual analysis of the TEM images. From those images we extracted the mean length of the ligands (oleic acid) and, since the ligands are the same for all the nanocrystals, we assumed it the same also for the green and the blue population. The as measured hydrodynamic diameters are: $11.8 \pm 1.7 \text{ nm}$ (red), $12.5 \pm 1.8 \text{ nm}$ (green) and $12.0 \pm 1.9 \text{ nm}$.

Electron microscopy

HAADF-STEM images, SE-STEM images, EDS maps and electron tomography series of the SPs were acquired using a FEI Osiris and a FEI Tecnai electron microscopes operated at 200 kV. Electron tomography series were acquired using a Fischione model 2020 single tilt tomography holder and the series were acquired within the tilt ranges from -64° to $+74^{\circ}$, from -76° to $+64^{\circ}$ and a tilt increment of 2° . Alignment of the tilt series was performed through cross-correlation routines⁷ implemented in Matlab. For the reconstruction of the series, the simultaneous iterative reconstruction technique (SIRT) was used, implemented in the ASTRA toolbox.⁸⁻¹⁰

HAADF-STEM images of the NCs were acquired using an aberration-corrected ‘cubed’ FEI Titan 60-300 electron microscope operated at 120 kV, equipped with a ChemiSTEM¹¹ system.

Radial distribution function

The radial distribution function of NC centers of mass in a SP was calculated from the reconstructed SP obtained from tomographic analysis. The individual NCs were automatically detected, and the center-of-mass coordinates extracted. Then the histogram of center-to-center distances was normalized to the distances in an ideal gas with the same density. In order to minimize the shape effects of the supraparticle, the volume of the droplet is approximated by the convex hull around all particle coordinates in the data set. The normalization factor is then calculated from the distances between centers-of-mass of an ideal gas in this volume, thus minimizing shape effects.

CIE diagram

The CIE coordinates of the different emitters were obtained firstly by multiplying the emission spectra with the standard color matching functions (CIE standard 1964). Then the tristimulus values (X , Y and Z) were obtained by integrating the previously calculated values over the entire visible spectrum. Finally, the CIE coordinates (x , y and z) were calculated from the tristimulus values using the following formulas:

$$x = \frac{X}{X + Y + Z} ; y = \frac{Y}{X + Y + Z} ; z = \frac{Z}{X + Y + Z}$$

The CIE coordinates, calculated in this way, and corresponding to the numbers in Fig. 5 of the main text, are as follow:

(0.1602; 0.7126; 0.1272)

(0.6767; 0.3233; 0.0001)

(0.1319; 0.1639; 0.7042)

(0.2666; 0.3599; 0.3735)

Packing fraction

The packing fraction of NCs in the SPs was determined by performing a thresholding of the reconstructed electron-density map of the SP through the Otsu method,¹² and comparing the thresholded volume with the overall volume of the assembly. This approach was chosen since no order of the single NCs was detected and since the particles do not have a spherical shape. The packing fraction measured this way was 0.8.

Figures

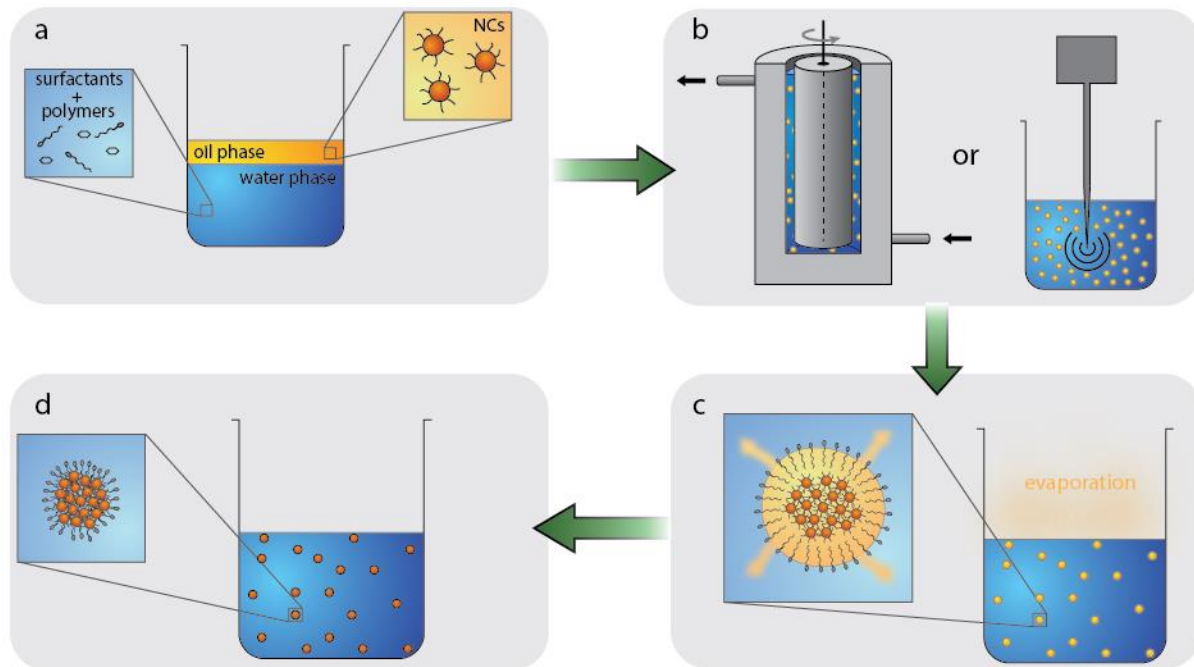


Figure S1: Schematic representation of the self-assembly procedure. **a**, The oil phase containing the NCs and the water phase containing surfactants, to stabilize the droplets, and polymers, to achieve a viscoelastic medium, are in contact forming a two phase system; **b**, the emulsification process can be performed in a Couette shear cell or *via* sonication; **c**, the oil phase of the droplets evaporates, thus forcing the contained NCs to self-assemble and form the SP; **d**, when all the oil phase is evaporated, the SPs are suspended in water due to a layer of surfactants.

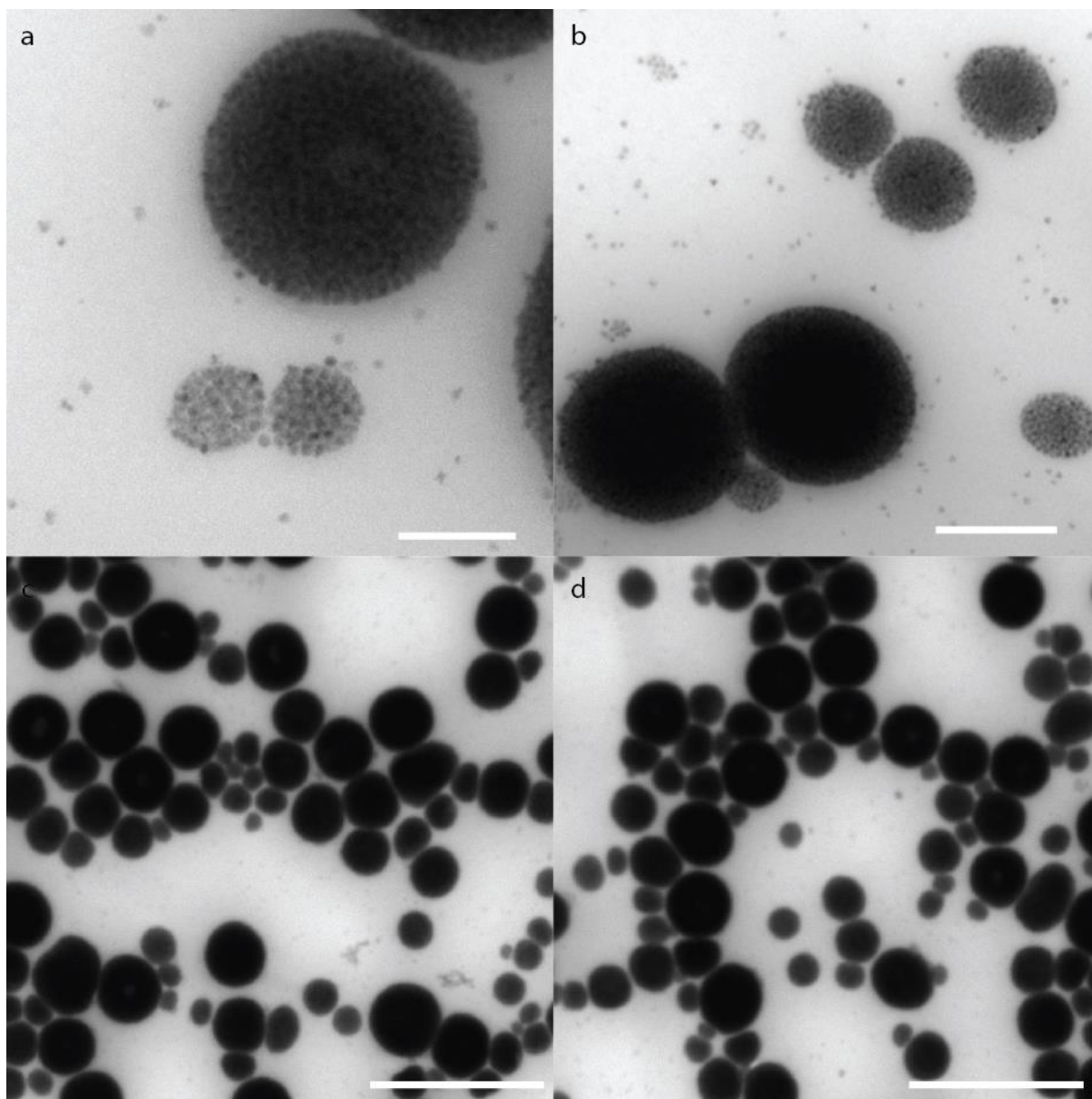


Figure S2: Representative bright field TEM images of different SPs. The non-spherical shape of some of the SPs in the image can be explained by an effect of the capillary forces during the drying process of the SPs from water on the TEM grid. Scale bars 100 nm (a), 200 nm (b), 1 μm (c-d).

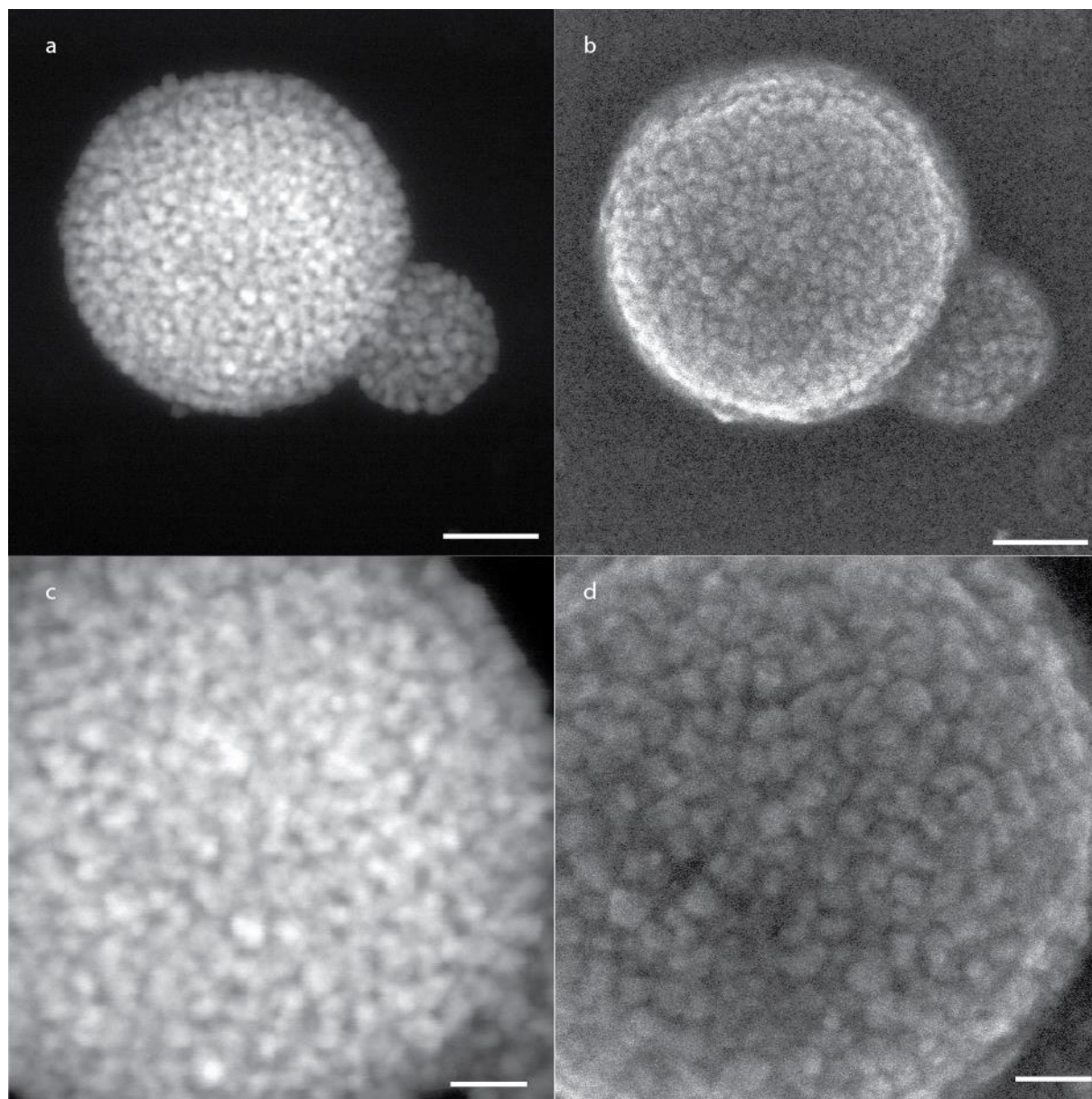


Figure S3: Representative SE-STEM and HAADF-STEM images of SPs. a, HAADF-STEM image of two SPs of different sizes (scale bar 50 nm). The small size is ideal to appreciate the inner structure of the SP and the arrangement of the NCs; **b**, SE-STEM of the same SPs of panel a (scale bar 50 nm). Thanks to the secondary electron detection, it is possible to observe the surface structure more in detail, such as the amorphous arrangement of the NCs; **c**, magnification of panel a (scale bar 20 nm); **d**, magnification of panel b (scale bar 20 nm).

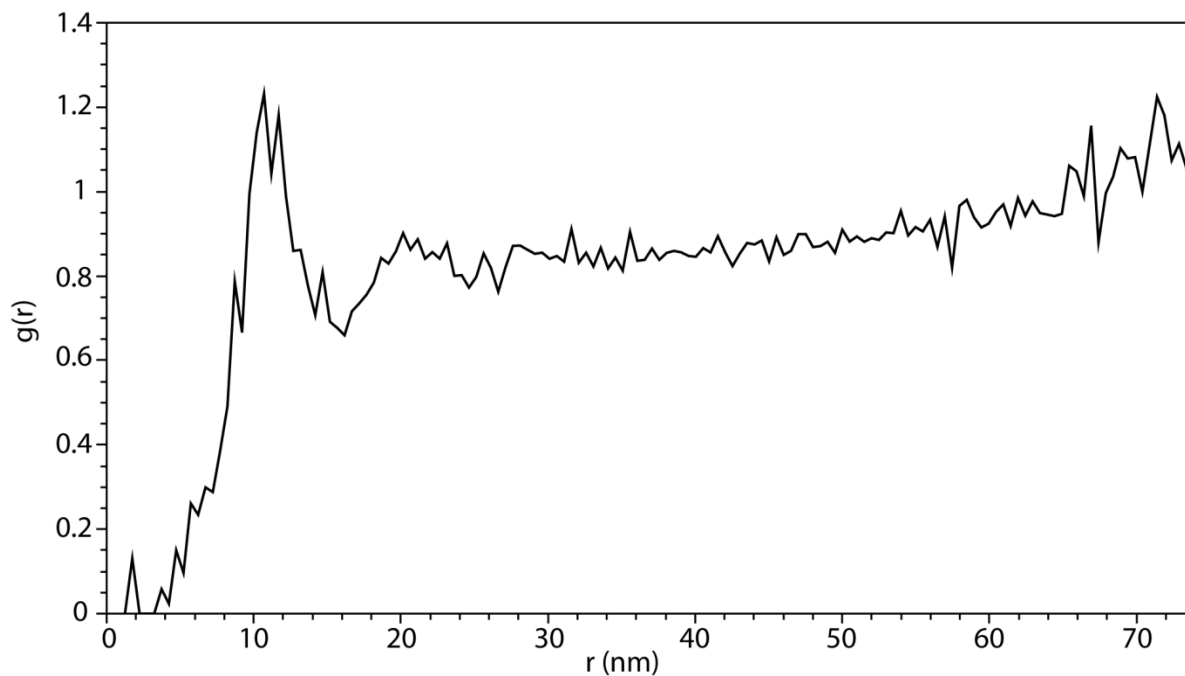


Figure S4: Radial distribution function calculated for the NC position in mixed SPs. The function shows an average distance between nearest neighbors of 10.9 nm, which is approximately equal to the average diameter of the NCs.

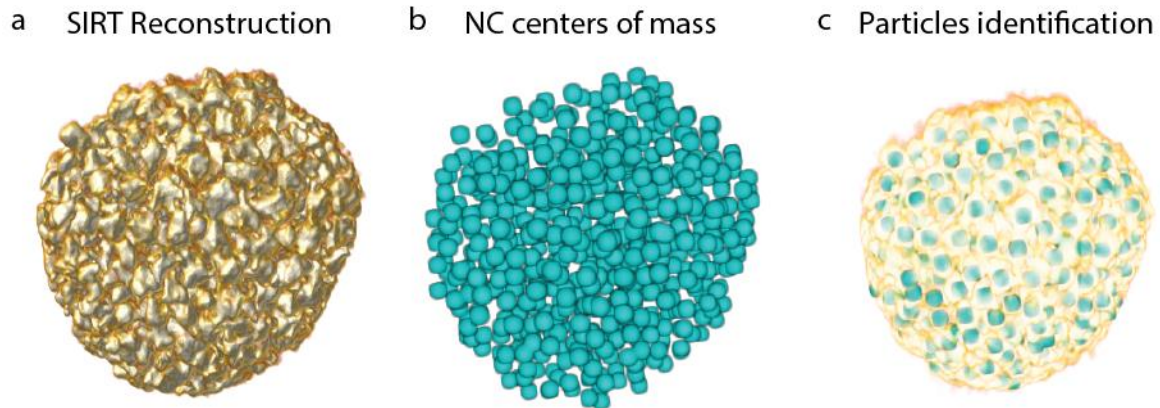


Figure S5: Obtaining the NC coordinates inside a SP. From HAADF-STEM imaging of the same SP under different tilt angles it is possible to reconstruct the inner structure of the SP. **a**, Volume rendering of the tomographic reconstruction obtained using the Simultaneous Iterative Reconstruction Technique (SIRT); **b–c**, Using the morphologies of individual NCs known from separate TEM images (*e.g.* Fig. S6, a-c), automatic segmentation can identify the centers of mass (**b**) and packing (**c**) of individual NCs in the SP.

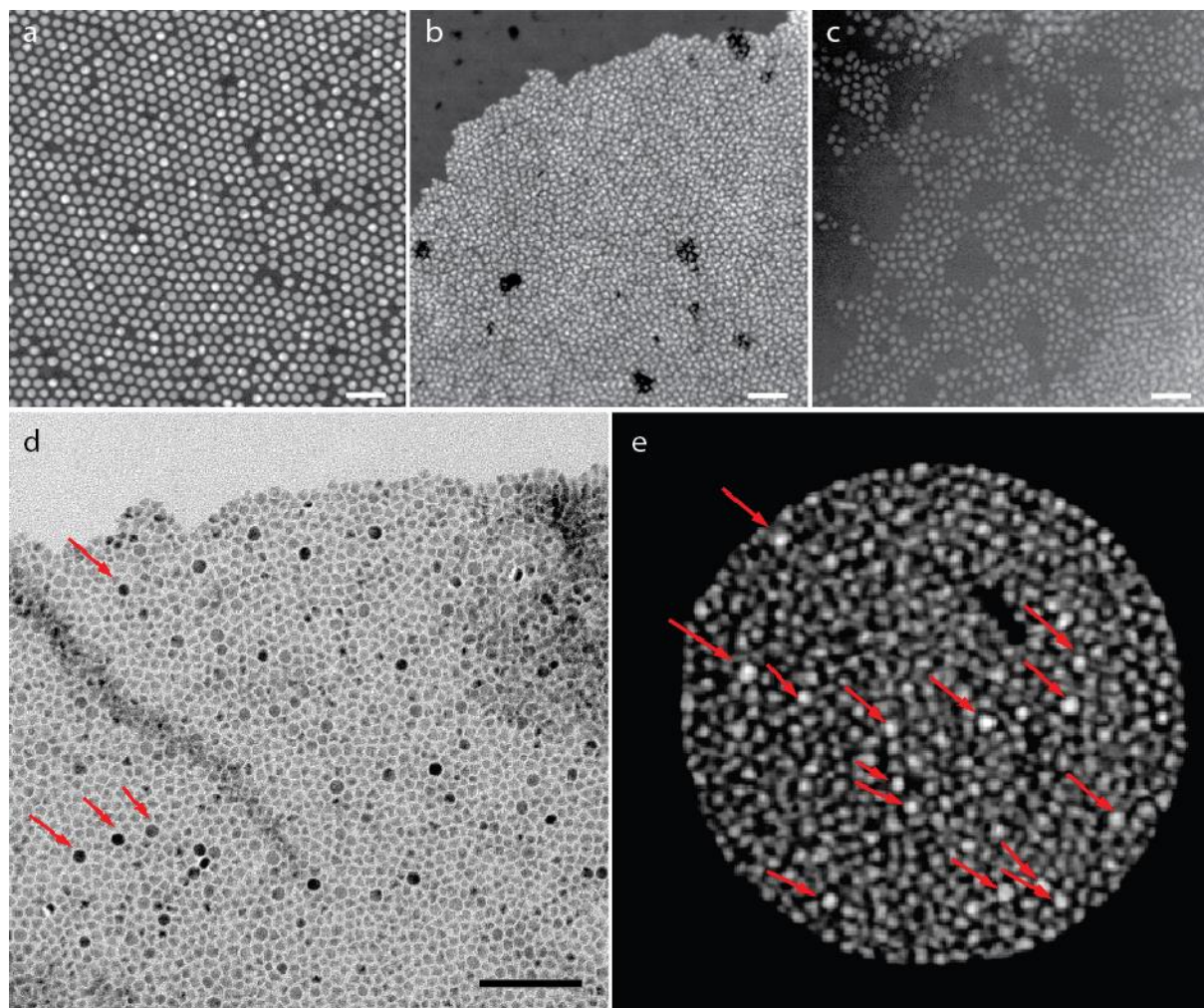


Figure S6: Identification of NCs inside the SP. **a**, HAADF-STEM image of the red population of NCs (scale bar 50 nm); **b**, HAADF-STEM image of the green population of NCs (scale bar 50 nm); **c**, HAADF-STEM image of the blue population of NCs (scale bar 50 nm); **d**, TEM image of the mixture of NCs used to make the SP on panel e, self-assembled on a liquid-air interface (scale bar 100 nm); some of the red NCs are highlighted with red arrows. Their regular and spherical morphology enables their identification over the irregularly branched green and blue NCs. The image clearly shows that the mixing of the different populations of NCs is homogeneous and no phase separation occurs in 2D; **e**, Orthoslice through one of the reconstructed SPs where it is possible to recognize some of the red NCs, indicated by red arrows. Also in 3D the NC populations mix homogeneously and no phase separation is observed.

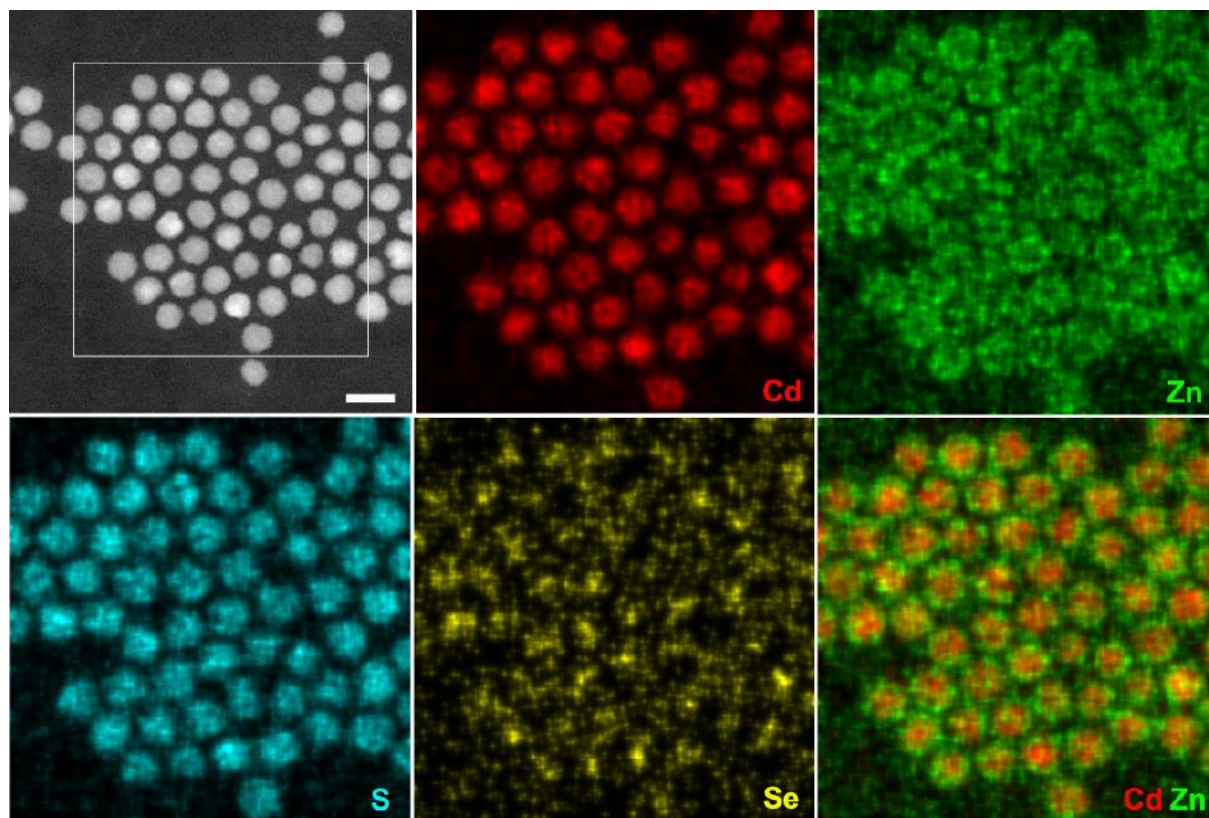


Fig. S7: Energy-Dispersive X-ray (EDS) maps of red emitting NCs, together with the corresponding HAADF-STEM image of the region used for the acquisition, revealing the distribution of the elements in the NCs.

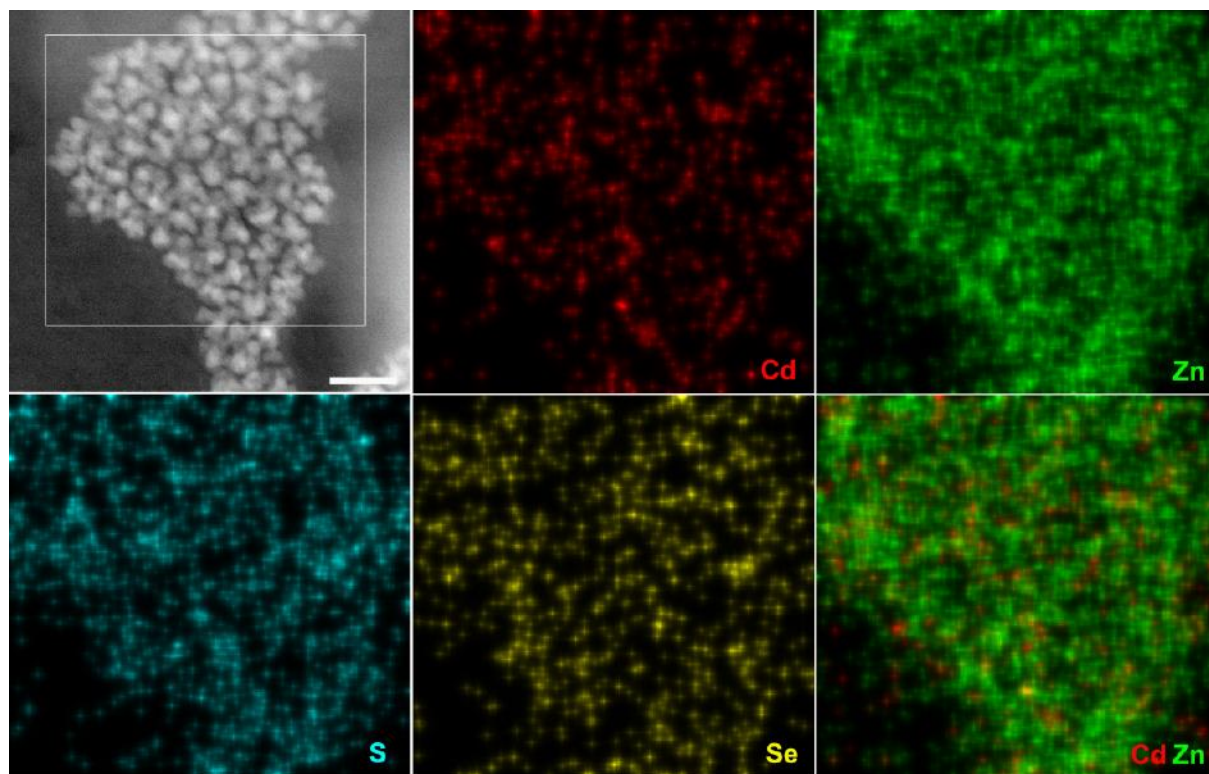


Fig. S8: Energy-Dispersive X-ray (EDS) maps of green emitting NCs, together with the corresponding HAADF-STEM image of the region used for the acquisition, revealing the distribution of the elements in the NCs.

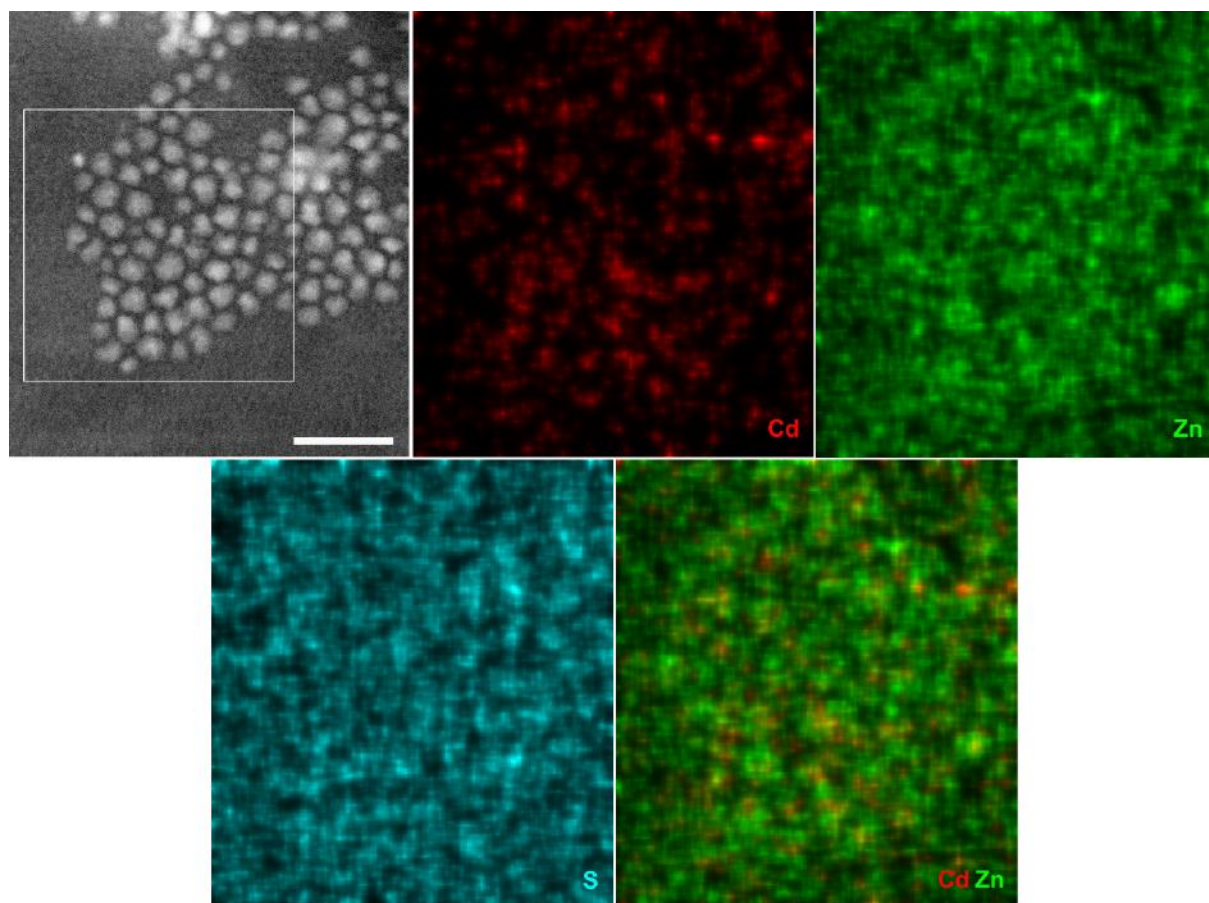


Fig. S9: Energy-Dispersive X-ray (EDS) maps of blue emitting NCs, together with the corresponding HAADF-STEM image of the region used for the acquisition. Instability of the sample under the electron beam hampered the acquisition of EDS maps with longer exposure time, therefore limiting the spatial resolution. In this case the maps were averaged to produce an overall composition measurement (Figure S10c).

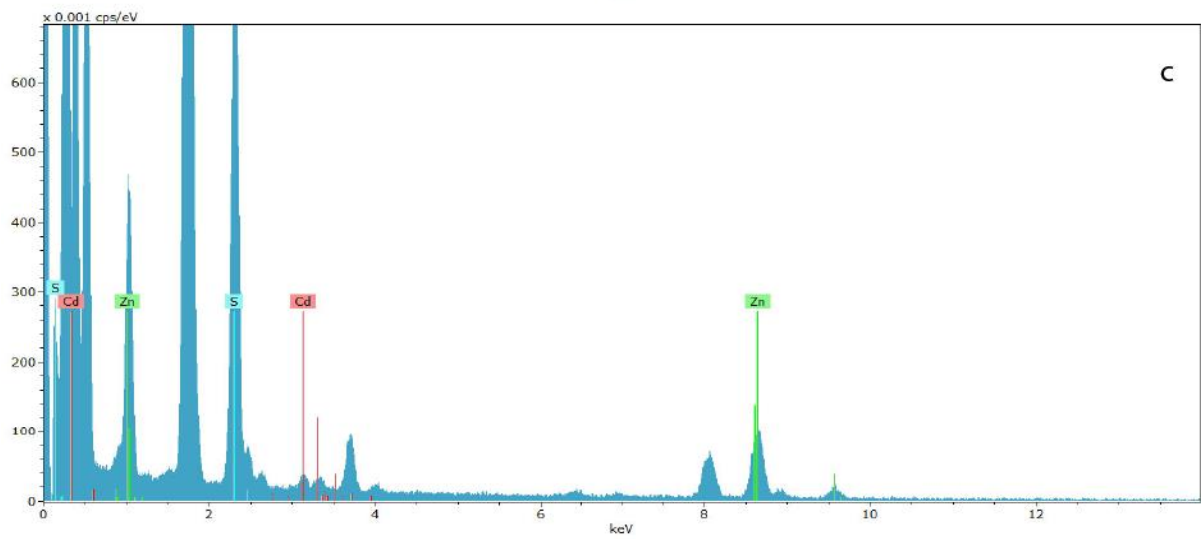
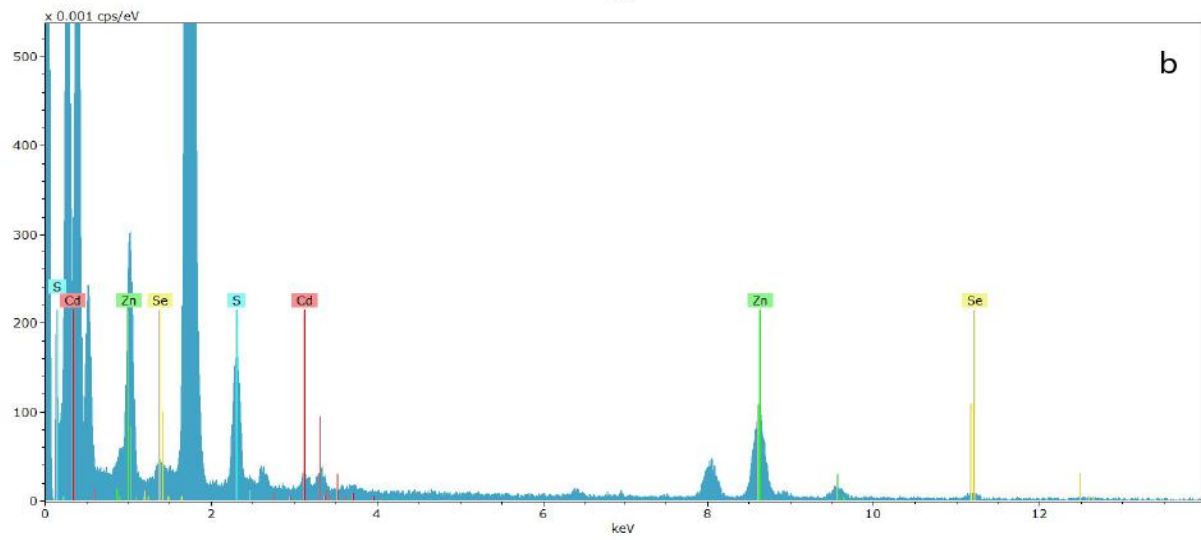
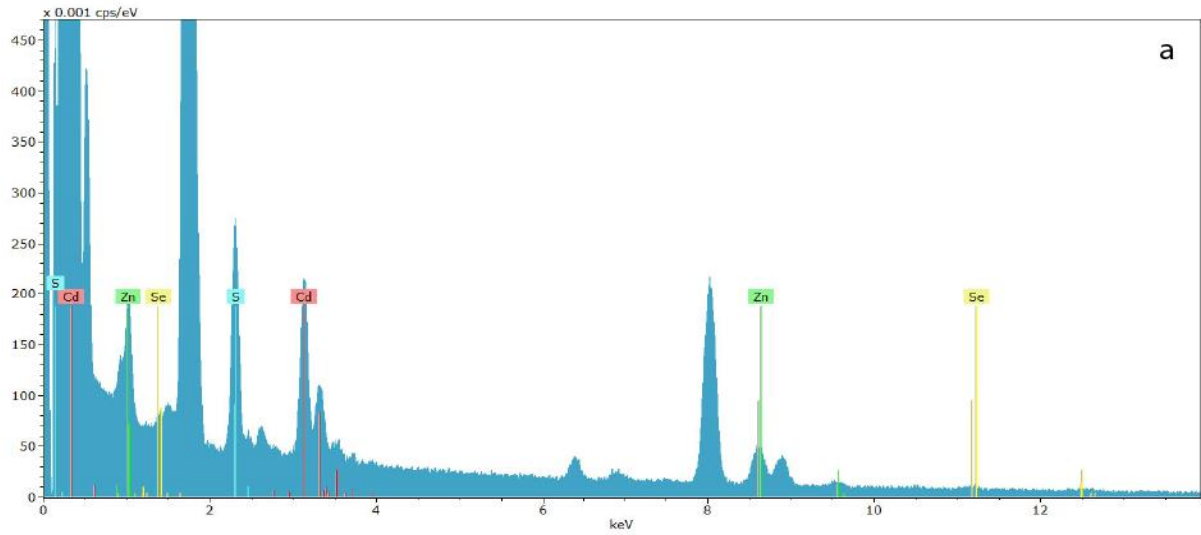


Fig. S10: Energy-Dispersive X-ray (EDS) spectra from the (a) red, (b) green and (c) blue NCs. The spectra were obtained by averaging the signal from the STEM-EDS maps shown in Figures S7-S9. It is clear that Cd concentration is a lot higher in the red crystals compared to the green and blue ones. The peaks at 1.7 keV and 8.1 keV which are not indicated correspond to Si and Cu originating from the SiN grid and the holder respectively.

	Red NCs	Green NCs	Blue NCs
Cd	63.7	13.9	8.2
Zn	13	53.7	27
S	22	26.5	64.8
Se	1.3	5.9	0

Table S1: Energy-Dispersive X-ray (EDS) quantification results. The mass % values of Cd, Zn, S and Se for the three different NCs are presented, as obtained from the spectra shown in Figure S10.

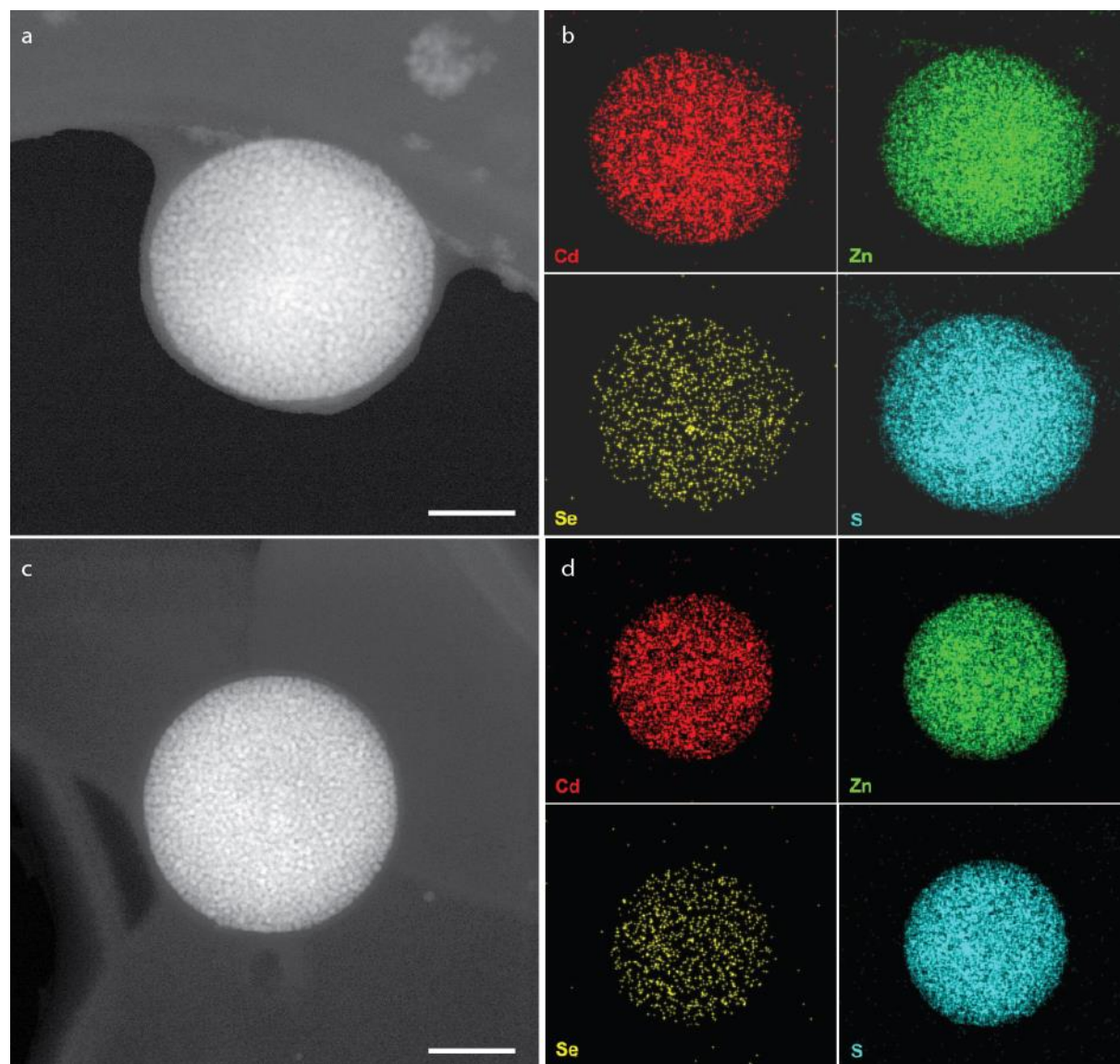


Figure S11: Energy-Dispersive X-ray (EDS) images of different SPs. (a,c) HAADF-STEM images of two different SP (scale bars 100 nm) composed of red, green, and blue emitting NCs, and (b,d) the corresponding energy-dispersive X-ray (EDS) maps for the elements Cd (red), Zn (green), Se (yellow), and S (blue). The EDS maps show that all elements are homogeneously distributed over the volume of the SPs, indicating homogeneous mixing of the NCs.

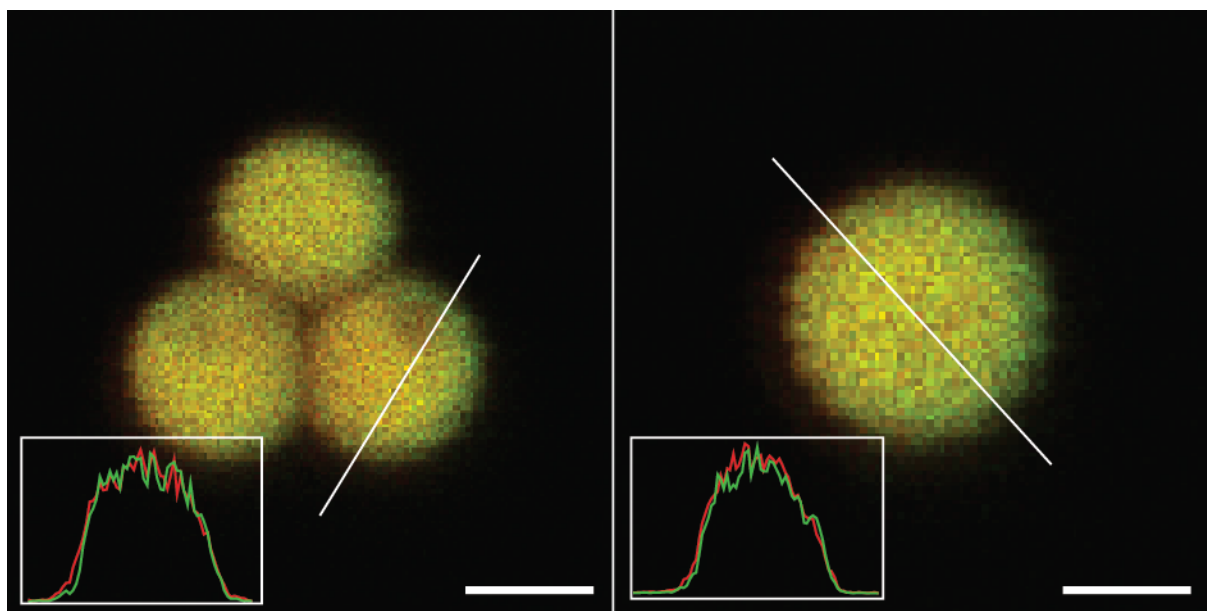


Figure S12: Confocal images showing the recorded emission of monodisperse SPs made of red, green and blue emitting NCs, deposited on a silicon wafer. The insets show the intensity profile of the emission in the blue/green spectral range (450-550 nm; green line) and in the red (600-700 nm; red line). Line profiles were taken over the straight lines indicated in the main images. Both color channels show similar emission profiles in terms of intensity and shape, indicating homogeneous mixing of the NCs in the SPs. Scale bars 1 μm .

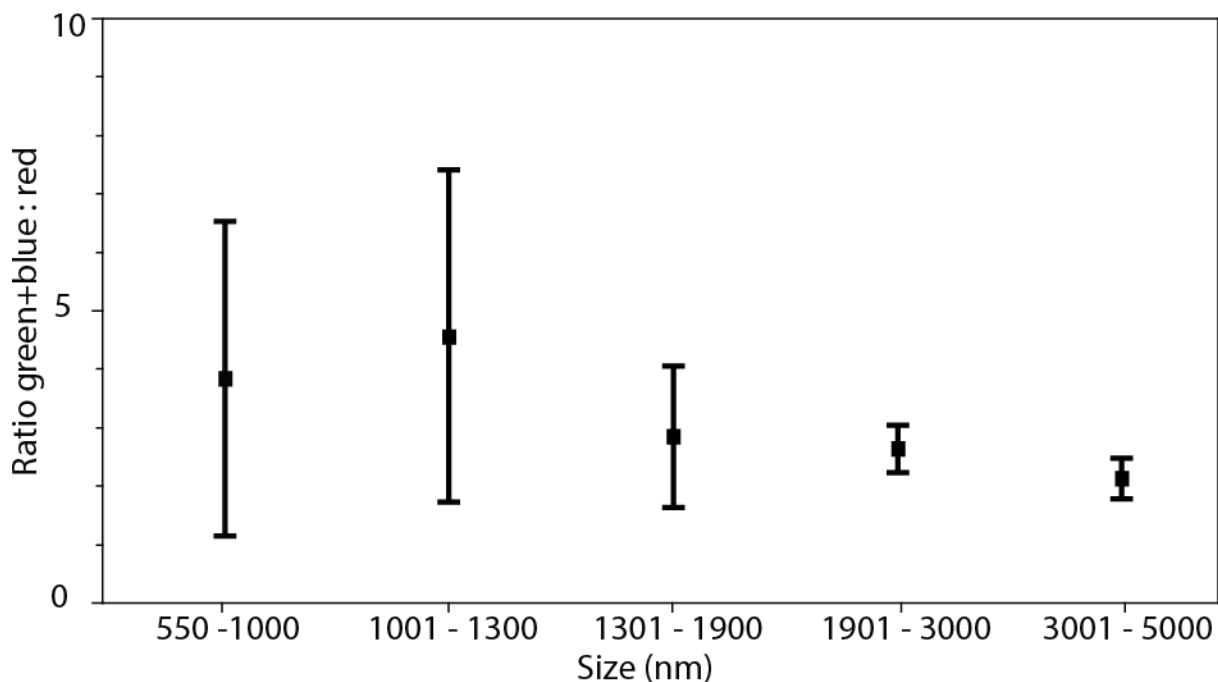


Figure S13: Analysis of the optical properties of single SPs through confocal imaging. The plot shows the ratio between the maximum of the green+blue peak and the maximum of the red peak in the emission spectra of the single SPs plotted *versus* their size. This plot supports the statement that the optical properties SPs are homogeneous throughout the synthesis batch, as the intensity ratio is similar for the different SP sizes. The relatively large error bars for sizes below 1300 nm are due to the close proximity between the volume of the SP and the volume of the PSF of the confocal microscope.

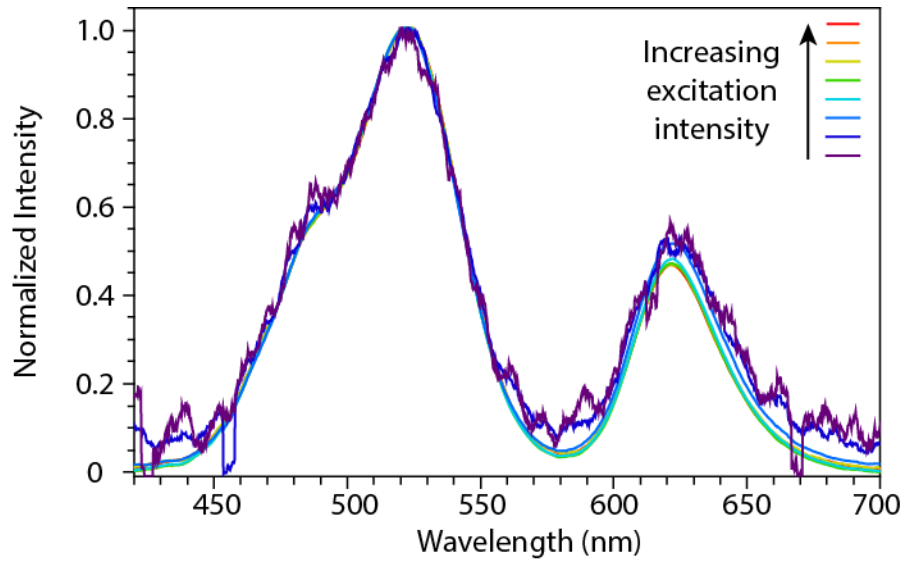


Figure S14: Emission spectra of a dispersion of SPs in function of the excitation power.

Emission spectra of a suspension of SPs in water excited with a diode laser at 405 nm at different excitation powers: 104.5 mW/cm² (red), 81.0 mW/cm² (orange), 62.1 mW/cm² (yellow), 42.4 mW/cm² (green), 18.9 mW/cm² (cyan), 1.7 mW/cm² (blue), 0.61 mW/cm² (dark blue), 0.036 mW/cm² (purple).

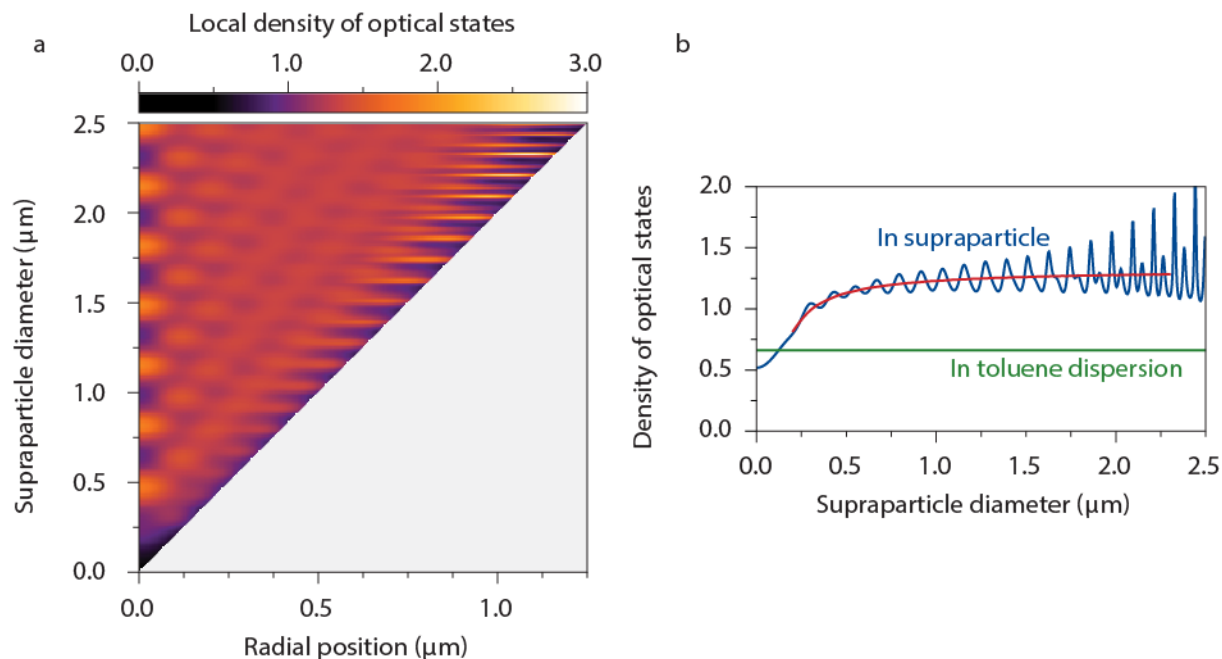


Figure S15: The local density of optical states in a supraparticle. **a**, We estimate the local density of optical states (LDOS) experienced by NCs in a SP using a simple model, by approximating the SP as a homogeneous dielectric sphere with a real refractive index. The LDOS in the SP, as a function of SP radius and radial position of the NC, can then be expressed as an expansion in terms of Mie coefficients.¹³ The plot shows the results for a red-emitting NC ($\lambda = 627$ nm) in a SP, averaged over transition-dipole orientation and normalized to the LDOS in vacuum. For the refractive index of the SP we take $n_{SP} = 1.89$ (= 50% CdS + 50% organic material/water with average $n = 1.4$) and for the environment we assume water ($n_{out} = 1.33$), as in the experiments of Figs. 4,5 of the main text. The “Mie” LDOS in the sphere is multiplied by a local-field correction factor $[3n_{SP}^2/(2n_{SP}^2 + n_{NC}^2)]^2$ to account for the locally higher refractive index of the NCs. **b**, The LDOS averaged over the volume of the SP (blue), compared to the LDOS experienced by a NC in toluene dispersion (green). In large (> 1 μm diameter) SPs the LDOS is approximately twice larger than in toluene dispersion (red; averaging out sharp Mie peaks using a Gaussian SP size distribution with 100 nm standard deviation).

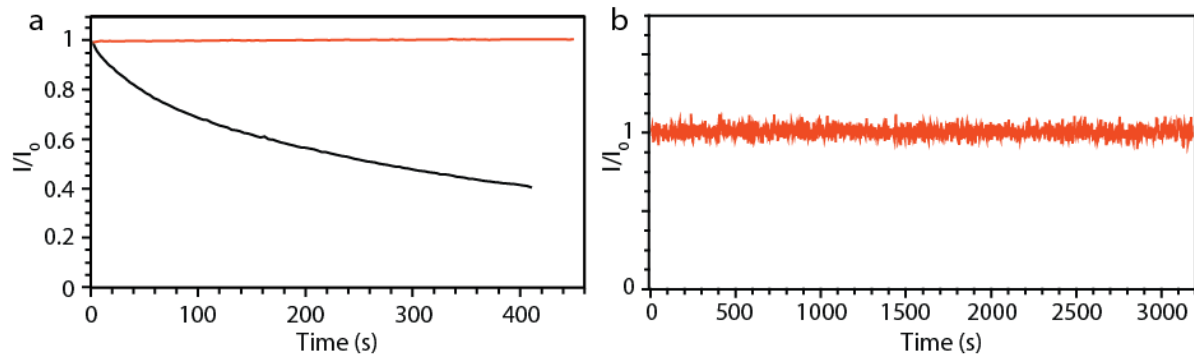


Figure S16: Photobleaching of Si particles filled with RITC compared to SPs. a, Photoluminescence emission intensity of a dispersion of SPs (red) and Si particles filled with rhodamine isothiocyanate (RITC) (black) over time under continuous excitation ($\sim 0.1 \mu\text{W}$ at 550 nm). The photobleaching of the latter one is evident from the graph; **b,** Representative photoluminescence emission trace of a single SP under continuous laser excitation.

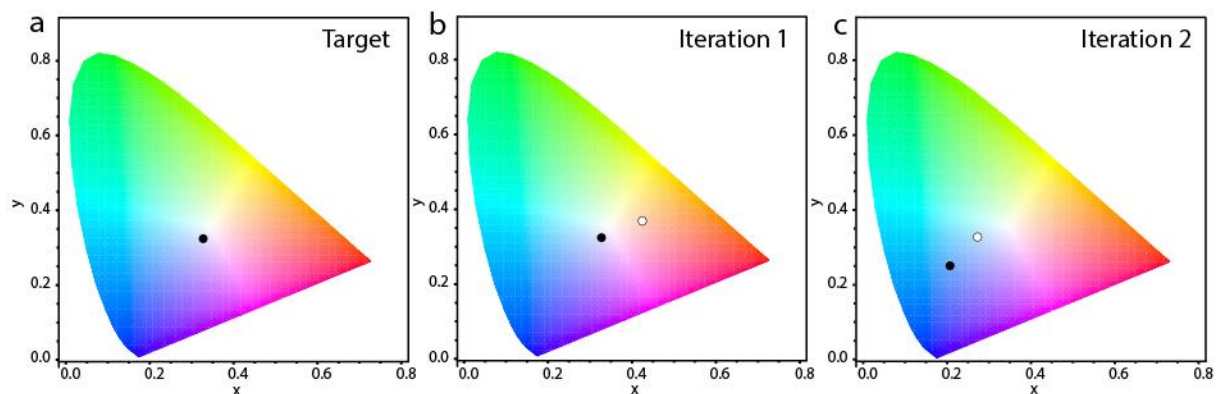


Fig. S17: Consecutive adaptations of the composition of the SPs to arrive at a given shade of white light, *i.e.* a given point in the CIE diagram. **a, we show here how one can approach the “bull’s eye” of the CIE diagram, indicated by the black point. **b**, we first prepare a solution of NCs with the target composition (black dot). The solution is then used to make SPs. From the emission spectrum of the SPs we find a considerable shift towards the red (white point). This is due to energy transfer and reabsorption events (see text). **c**, Then we prepare a new solution of NCs taking in account the shift of step 1 (black dot). The new adapted solution is used to make SPs. The resulting SPs have CIE coordinates much closer to the target point compared to step 1 (white point). With some iterations, one can fabricate SPs with precisely the desired emission spectrum.**

References

- (1) Li, J. J.; Wang, Y. A.; Guo, W.; Keay, J. C.; Mishima, T. D.; Johnson, M. B.; Peng, X. Large-Scale Synthesis of Nearly Monodisperse CdSe / CdS Core / Shell Nanocrystals Using Air-Stable Reagents *via* Successive Ion Layer Adsorption and Reaction. *J. Am. Chem. Soc.* **2003**, 933–937.
- (2) Ki Bae, W.; Kwak, J.; Park, J. W.; Char, K.; Lee, C.; Lee, S. Highly Efficient Green-Light-Emitting Diodes Based on CdSe@ZnS Quantum Dots with a Chemical-Composition Gradient. *Adv. Mater.* **2009**, 21, 1690–1694.
- (3) Lee, K.; Lee, J.; Song, W.; Ko, H.; Lee, C.; Lee, J.; Yang, H. Highly Efficient, Color-Pure, Color-Stable Blue Quantum Dot Light-Emitting Devices. *ACS Nano* **2013**, 7295–7302.
- (4) Mason, T. G.; Bibette, J. Shear Rupturing of Droplets in Complex Fluids. *Langmuir* **1997**, 13, 4600–4613.
- (5) Mabile, C.; Schmitt, V.; Gorria, P.; Leal Calderon, F.; Faye, V.; Deminière, B.; Bibette, J. Rheological and Shearing Conditions for the Preparation of Monodisperse Emulsions. *Langmuir* **2000**, 16, 422–429.
- (6) Besseling, T. H.; Jose, J.; van Blaaderen, A. Methods to Calibrate and Scale Axial Distances in Confocal Microscopy as a Function of Refractive Index. *J. Microsc.* **2015**, 257, 142–150.
- (7) Guizar-Sicairos, M.; Thurman, S. T.; Fienup, J. R. Efficient Subpixel Image Registration Algorithms. *Opt. Lett.* **2008**, 33, 156–158.

- (8) van Aarle, W.; Palenstijn, W. J.; Cant, J.; Janssens, E.; Bleichrodt, F.; Dabravolski, A.; Beenhouwer, J. De; Batenburg, K. J.; Sijbers, J. Fast and Flexible X-Ray Tomography Using the ASTRA Toolbox. *Opt. Express* **2016**, *24*, 25129–25147.
- (9) van Aarle, W.; Palenstijn, W. J.; De Beenhouwer, J.; Altantzis, T.; Bals, S.; Batenburg, K. J.; Sijbers, J. The ASTRA Toolbox: A Platform for Advanced Algorithm Development in Electron Tomography. *Ultramicroscopy* **2015**, *157*, 35–47.
- (10) Palenstijn, W. J.; Batenburg, K. J.; Sijbers, J. Performance Improvements for Iterative Electron Tomography Reconstruction Using Graphics Processing Units (GPUs). *J. Struct. Biol.* **2011**, *176*, 250–253.
- (11) Schlossmacher, P.; Klenov, D. O.; Freitag, B.; von Harrach, H. S. Enhanced Detection Sensitivity with a New Windowless XEDS System for AEM Based on Silicon Drift Detector Technology. *Micros. Today* **2010**, *18*, 14–20.
- (12) Otsu, N. A Threshold Selection Method from Gray-Level Histograms. *IEEE Trans. Syst. Man. Cybern.* **1979**, *9*, 62–66.
- (13) Chew, H. Radiation and Lifetimes of Atoms inside Dielectric Particles. *Phys. Rev. A* **1988**, *38*, 3410–3416.